

Coagulation Kinetics of Humic Aggregates in Mono- and Di-Valent Electrolyte Solutions

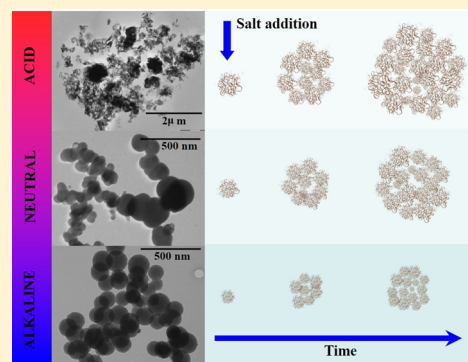
Long-Fei Wang,[†] Ling-Ling Wang,[†] Xiao-Dong Ye,^{‡,*} Wen-Wei Li,[†] Xue-Mei Ren,[§] Guo-Ping Sheng,[†] Han-Qing Yu,^{†,*} and Xiang-Ke Wang[§]

[†]Department of Chemistry, [‡]Department of Chemical Physics, University of Science & Technology of China

[§]Institute of Plasma Physics, Chinese Academy of Sciences, Hefei, 230026, China

Supporting Information

ABSTRACT: Coagulation behaviors of humic acids (HAs) aggregates in electrolyte solutions at different pHs, valences and concentrations of electrolyte cations were investigated using dynamic light scattering technique in combination of other analytical tools. For monovalent electrolyte sodium chloride (NaCl) solution, at its low concentrations the average hydrodynamic radius ($\langle R_h \rangle$) of aggregates kept nearly constant. However, at high NaCl concentrations, $\langle R_h \rangle$ could be scaled to the time t as $\langle R_h \rangle \propto t^a$, suggesting a diffusion-limited colloid aggregation (DLCA). The coagulation value of NaCl in a buffer at pH 7.1 was calculated to be in a range of 61.3–84.4 mM. Divalent cation Mg^{2+} was far more effective in enhancing the HA coagulation, as evidenced by a lower coagulation value (between 1.0 and 1.7 mM) and a more rapid coagulation rate. Such an enhancement could be explained by the combined effects of electrostatic repulsion, complexation and bridging. The highest coagulation rate ($d\langle R_h \rangle/dt$) and coagulation value at different pHs followed the order of: acidic > neutral > alkaline, and alkaline > neutral > acidic, respectively. Such a difference was associated with the extent of hydrogen bond and electrostatic repulsion at different protonation/deprotonation states of carboxyl and phenolic –OH groups. Transmission electron microscopic imaging reveals that HA was predominantly globular aggregates with a rough periphery at pH 5.26, and was changed to smooth spherical particles at pH 10.00. These results are useful for better understanding the coagulation behaviors of HAs in both natural and engineered aqueous systems.



INTRODUCTION

Humic substances (HS) are formed from biochemical weathering of plants and animal remains and are widely present in nature.^{1,2} As a principal component of HS, humic acid (HA) has many unique properties, for example, insoluble at pH < 2, but soluble at higher pHs, and has been implicated in both engineered and natural processes. One promising application direction is for environmental pollutant removal and a profound impact of HA on the transport, sequestration, and mitigation of environmental contaminants has been well recognized.^{2–4} Especially, HAs tend to coagulate, and the aggregated HA molecules are found to trap a considerable amount of contaminants and thus weaken the degradation and neutralization of contaminants.⁴ In addition, the colloidal aggregates of HA confer excess potential binding sites for many materials, for example, metals, clay particles, and pesticides.⁴ Apparently, the coagulation of HAs remarkably influences their interactions with contaminants in aqueous/soil systems and is of great significance for environmental remediation. Thus, an exploration into the coagulation mechanisms of HA has attracted intensive interests worldwide.

The aggregation/coagulation of HAs has been studied with several techniques, for example, fluorescence spectroscopy,⁵ atomic force microscopy,⁶ turbidity,⁷ fluorescence correlation

spectroscopy,^{3,8,9} capillary zone electrophoresis,¹⁰ nuclear magnetic resonance,¹¹ surface tension measurements,^{12,13} and dynamic light scattering (DLS).^{14–16} For example, the fluorescence correlation spectroscopy revealed that the disaggregation rate of HA particles was strongly dependent on pH.³ Among these techniques, DLS offers a powerful tool to determine the size distribution of nanoparticles in suspension and polymers in solution and has been used to explore the size, fractal characteristics, and coagulation kinetics of HAs.^{14–17}

The physicochemical properties of HAs, such as their inherent biopolymer chain structure and colloidal characteristics, are related highly to the solution chemistry, for example, electrolyte and pH. The ionized and un-ionized states of functional groups including carboxyl and phenolic –OH, which vary considerably with pH change, significantly influence metal complexation, surface charge, and supramolecular structure.^{4,18–20} For example, formation of negative charges due to ionization of carboxyl groups is responsible for the mutual repulsion and expansion of coil.¹⁸ It is found that electrostatic

Received: December 20, 2012

Revised: April 8, 2013

Accepted: April 17, 2013

Published: April 17, 2013

interactions play a predominant role in the colloidal stabilities of HA and that its aggregation is governed mainly by the screened electric field developed from the dissociation of acidic groups bound to the cross-linked polymeric network of HA molecules.²¹ Theoretical explanations for the sensitivity of colloidal stability as a function of pH and electrolyte have also been provided.²² Na⁺ and Mg²⁺ are among the most abundant cation ions in natural waters²³ and HA can cause severe membrane fouling problems in engineered filtration processes.^{24,25} An investigation into the coagulation of HA in electrolyte solutions might aid a better understanding of the membrane fouling caused by HA in seawaters as well as in freshwaters, especially in the case of eutrophication.^{24–26} The condensed HS at acidic-pH landfill leachates and mining effluents may significantly affect a wide range of geochemical processes, such as humic–metal complexation and pollutant detoxification.²⁷

However, so far most studies concerning HA aggregation/coagulation were conducted under equilibrium or near equilibrium conditions.^{3,5–8,10–13} The HA coagulation kinetics and the effects of cation valence and solution pH on HA coagulation behaviors (e.g., coagulation kinetics, rate of early stage, and final aggregate size) have not been thoroughly understood yet.

In this work, DLS analysis was performed to explore the coagulation behaviors of HA in monovalent and divalent electrolyte solutions. The chemical elements, functional groups, structure information were comprehensively identified using combined techniques, including Fourier transform infrared (FTIR) spectroscopy, X-ray photoelectron spectroscopy (XPS) and acid–base titration. Typical monovalent (NaCl) and divalent (MgCl₂) electrolytes were applied to induce coagulation of HA in buffers at different pHs. The coagulation kinetics in the presence of NaCl at pH 7.1 was fitted with typical diffusion-limited colloid aggregation (DLCA) model. The coagulation behavior of HAs governed by solution chemistry was examined in terms of their colloidal properties, and was elucidated from a physical chemistry point of view. In addition, transmission electron microscope (TEM) was used to image the morphology of HA colloids.

MATERIALS AND METHODS

HA and Solutions. AR-grade electrolytes (NaOH, HCl, NaCl, and MgCl₂) at various concentrations were prepared and filtered with 0.22 μm filter prior to use. Buffers used in this study were prepared with Millipore water according to Rex et al.: glycine-HCl for pH 3.6, Tris-HCl for pH 7.1, and glycine-NaOH for pH 10.0.²⁸

Commercial HAs purchased from North China Chemical Reagent Co., China, were purified¹ prior to use as a model to study the coagulation behaviors of natural organic materials. 10 g of HA was dissolved in 1 L of 0.1 M NaOH and then filtered. The solution was acidified to pH 1.0 using concentrated HCl solution and filtered. The precipitates were washed with 0.1 M HCl for three times and lyophilized. Such purified HAs were dissolved in buffers to reach a final concentration of 100 mg L⁻¹ and left for 12 h to reach complete dissociation.

XPS, FTIR, Acid–Base Titration. XPS (ESCALABMKII, VG Co., UK) was used to examine the elemental compositions and functional groups. Survey and high-resolution scans were collected using pass energies of 20.0 and 70.0 eV, in which the broad survey scan (20.0 eV pass energy) was conducted for

major element compositions and the high-resolution scan (70.0 eV pass energy) for component speciation.

FTIR measurements were carried out with VERTEX 70 FTIR (Bruker Co., Germany). For each sample, approximately 5 mg of HA was dissolved in Millipore water. The solution pH values were adjusted to 1.70, 5.25, and 10.04 with 0.2 M HCl and NaOH solutions, respectively. Lastly, the samples were mixed with KBr powder for FTIR analysis after lyophilization.

Acid–base titration was carried out using an automated titrator (DL50 Mettler-Toledo Inc., Switzerland) at 25 °C. HA at a concentration of 1250 mg L⁻¹ was dissolved in Millipore water. Before titration, a given amount of 0.1 M HCl was added to lower the pH to below 3.0. The solution was initially stirred for 20 min and then titrated with 0.09 M NaOH solution under N₂ atmosphere programmed in incremental monotonic mode with a dosing unit of 8 μL. The titration data acquired were analyzed with the PROTOFIT 2.1 software by using the Donnan Shell Model.²⁹ The titration results were also compared with the NICA (nonideal competitive adsorption)–Donnan simulations of reported HAs detailed in Supporting Information (SI).

DLS and Electrophoretic Mobility. DLS measurements were conducted using an ALV/DLS/SLS-5022F spectrometer equipped with a multi-τ digital time correlator (ALV5000), and a cylindrical 22 mW UNIPHASE He–Ne laser (λ₀ = 632.8 nm) as the light source at 25 °C. The glass vials (27150-U, Supelco Co., Bellefonte, PA) used were cleaned in piranha solution (1:3 vol/vol of 30% hydrogen peroxide and concentrated sulfuric acid) and then thoroughly leached with distilled acetone. For each sample, 2 mL of HA solution at a concentration of 100 mg L⁻¹ in designed buffers was filtered into one dust-free vial with a 0.45 μm hydrophilic PTFE (Millipore Millex-LCR) and left overnight. A certain amount of electrolyte solution with diverse concentrations was filtered into the HA solution. The vial was placed in a sample holder without further stirring and the scattered light intensity was adjusted before each measurement. The weights before and after the dose of electrolyte solution were recorded so that the exact electrolyte concentration in each vial could be calculated.

The scattering angle was set at 90° and duration of a single measurement was 30 s. In DLS, the Laplace inversion of a measured intensity–intensity time correlation function $G^{(2)}(t, q)$ in the self-beating mode can result in a line-width distribution $G(\Gamma)$ by CONTIN method. For a pure diffusive relaxation, Γ is related to the translational diffusion coefficient D by $\Gamma/q^2 = D$ at $q \rightarrow 0$ and $C \rightarrow 0$. In this study, no extrapolation of $q \rightarrow 0$ and $C \rightarrow 0$ was done and an apparent hydrodynamic radius $R_h = k_B T / (6\pi\eta D)$ was determined, with k_B , T , and η being the Boltzmann constant, absolute temperature, and solvent viscosity, respectively.³⁰ As the scattered light intensity should be adjusted before each experiment, the time between the injection of electrolyte solution and first measured value was controlled close to 120 s. The coagulation kinetics was examined without stirring. In addition, the measured correlation functions were also analyzed by the cumulant method, and the two methods showed similar results. The polydispersity indexes (PDI) derived from the cumulant analysis were less than 0.3, indicating the results were fairly reliable.³¹

The electrophoretic mobility of each sample was recorded using a Nanosizer ZS instrument (Malvern Instruments Co., UK) equipped with backscattering detection at 173° and 25 °C. HA was dissolved in pH 7.1 Tris-HCl buffer to reach a final

concentration of 200 mg L⁻¹. HA solution and NaCl solution at different concentrations were mixed at equal volume and measured. Each sample was measured at least 6 times and data were presented as mean \pm standard deviation.^{32,33}

Coagulation Kinetics Analysis. According to the classical DLVO theory, the energy of interaction between two approaching particles plays a key role in coagulation.³⁴ Two regimes of irreversible colloid aggregation, that is, reaction-limited colloid aggregation (RLCA) and diffusion limited colloid aggregation (DLCA), have been identified. DLCA occurs when there is negligible repulsive force (e.g., in solutions at a high electrolyte concentration) and the aggregation rate is limited solely by the time taken for clusters to encounter each other by diffusion.^{34,35} On the other hand, RLCA occurs when there is a substantial but not insurmountable repulsive force between particles.^{35,36}

The coagulation process can be reasonably described by a power-law equation as a function of time, that is, $R \propto t^a$ in DLCA regime, and an exponential equation in RLCA regime.^{35–37} The reverse of the exponent is defined as the mass fractal dimension ($d_f = 1/a$), which can be used to describe the scaling behavior of highly disordered structure of colloidal aggregates.^{36,38} The d_f reflects the actual space occupied by the system and characterizes the degree of “openness” of the fractal structure.³⁹ Any object in a real physical process must have a mass fractal dimension $1 \leq d_f \leq 3$. A lower d_f means that the penetration of particles into a fractal cluster is more efficient. The typical mass fractal dimension is $d_f \approx 1.8$ for DLCA, and $d_f \approx 2.1$ for RLCA, indicating a more compact structure in RLCA.^{35,39}

TEM Observation. To prepare TEM images, the HA powders were dissolved in Millipore water to a concentration of 100 mg L⁻¹. Then, the pH values were adjusted to 5.26, 7.00, and 10.00 with dilute HCl and NaOH solutions, respectively. Several drops of each sample were added onto copper grids. To ensure the HA colloids to keep their original morphology to the largest extent, copper grids were instantly frozen in liquid nitrogen, followed by lyophilization.

RESULTS

Physicochemical Properties of HA. The XPS results show that the elemental composition of C, O, N, and S were 69.80%, 24.99%, 4.88%, and 0.33%, respectively. The detailed XPS analysis results are provided in SI Figure S1 and Table S1. The FTIR spectra of HAs show typical functional groups in SI Figure S2 and the assignments given to the various bands are tabulated in SI Table S2. By comparison, one significant difference between the spectra was the loss of the –COOH band at 1720 cm⁻¹ in alkaline solution as a result of deprotonation of –COOH.^{1,40} Peak intensity in a range of 1280–1200 cm⁻¹ reflected the extent of H-bonds,⁴⁰ whereas the reduction of intensity at pH 10.04 corresponded to the deprotonation of H-bonds.

In HS-related studies, the concentrations of main functional groups, that is, carboxyl and phenolic –OH, have been measured and reported.^{41,42} From the titration data, the Donnan shell model with two discrete sites was applied to simulate our results.²⁹ The pK values of carboxylic and phenolic –OH groups were estimated to be 5.08 and 7.96. The site densities were calculated to be 3090 and 1050 mmol kg⁻¹_{dw} for the carboxylic and phenolic –OH groups, respectively (SI Table S3). The titration data were generally in agreement with

the NICA-Donnan simulation results of the reported HA (SI Figure S3).

HA Coagulation in NaCl Solution. Figure 1 illustrates the $\langle R_h \rangle$ changes of HA aggregates as a function of time and NaCl

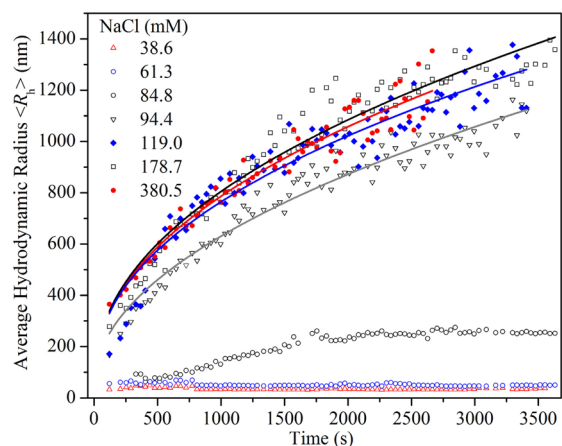


Figure 1. Coagulation profiles of HA aggregates as a function of time over a range of NaCl concentration from 38.6 mM to 380.5 mM at pH 7.1.

concentration. At a low concentration of NaCl (0–61.3 mM), $\langle R_h \rangle$ remained about 50 nm, indicating the stability of HA colloids. The z-mean of the square of the radius of gyration (R_g) of HA molecules is reported to be 4–10 nm,¹⁹ much smaller than the size of the stable HA colloids (52 nm) in this study. In a similar work, Pinheiro et al. reported initial aggregate sizes for peat HS in a range of 30–185 nm.¹⁴ Thus, HA colloids can be regarded as an entity of small aggregates here. When the NaCl concentration was further increased from 84.8 to 380.5 mM, the stability of colloids was destroyed. Ultimately, coagulation occurred as indicated by the rise of $\langle R_h \rangle$.⁴³ The characteristic aggregate sizes in each profile were applied to fit with typical power-law function of the DLCA regime to obtain the most optimum coagulation kinetics. The fitting details are given in Table 1. The initial $\langle R_h \rangle$ was fixed as the average value of 52 nm in the presence of 61.3 mM NaCl.

Table 1. Coagulation Kinetics for HA in Tris-HCl Buffer (pH 7.1)

NaCl (mM)	optimum kinetics ($R_0 = 52$ nm)	parameters			adjusted R^2	regime
		a	b	d_f (fractal dimension)		
94.4	$R = b \cdot t^a + R_0$	0.50	18.0	2.00	0.957	DLCA
119.0		0.44	33.1	2.27	0.914	
178.7		0.46	32.4	2.17	0.940	
380.5		0.45	31.9	2.22	0.942	

To test the variations of $\langle R_h \rangle$ in coagulation, the time-dependent hydrodynamic radius distributions $f(R_h)$ were calculated by CONTIN algorithm. The results are shown in Figure 2, taking the 119 mM NaCl profile as an example. The shift of the peak indicates the growth of HA colloid size in coagulation.⁴⁴ It is worth noting that a broader distribution means a larger difference in $\langle R_h \rangle$.³⁰ The width of the distribution function increases as a function of time, which is consistent with the observation in Figure 1, in which HA

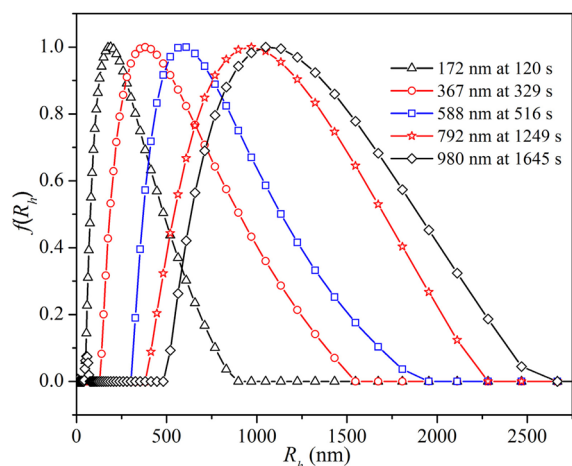


Figure 2. Time-dependent hydrodynamic radius distributions $f(R_h)$ for HAs in 119 mM NaCl solution at pH 7.1.

aggregates were found to exhibit more randomly fluctuating $\langle R_h \rangle$ at later stages. At the final coagulation stage, also called quasi-steady state, aggregates continued to grow at a slower rate than the early linear growth stage. This coagulation progress was likely governed by larger aggregate-aggregate interactions and collisions, resulting in a much wider distribution of $\langle R_h \rangle$.⁴⁴

Coagulation value is defined as the minimum concentration of the electrolyte required to cause coagulation of colloids.³⁴ Figure 1 shows that the coagulation value was in a range of 61.3–84.8 mM. HA coagulation in acidic and alkaline buffers (pH 3.6 and 10.0) induced by NaCl was investigated (Figure 3 and SI Figure S4). At pH 3.6, HA quickly coagulated at a rather low NaCl concentration. In alkaline solution, more electrolytes were needed to induce the coagulation, confirmed by the highest coagulation value (116.0–127.6 mM). Considering the background ionic strength of buffer solutions, the coagulation values of the three solutions were in the order of: alkaline > neutral > acidic. For each pH, a typical coagulation profile was selected to represent the early coagulation rate of HA (Table 2). The typical coagulation rate at pH 3.6 was almost an order of magnitude higher than that at pH 10.0 even at a much lower electrolyte concentration (22.4 mM compared to 127.6 mM). In a similar work to evaluate the influence of pH on HA diffusion coefficient,¹⁴ Pinheiro et al. found that at pH < 2.5, coagulation occurred quickly, leading to the precipitation of HA. A noticeable decrease in size was observed after pH was increased from 4.0 to 6.0.¹⁴ A significant variance was also observed for the final maximum aggregate $\langle R_h \rangle$, which decreased from 1452 nm at pH 3.6 to 528 nm at pH 10.0 (Table 2).

HA Coagulation in MgCl₂ Solution. To evaluate the effect of cation valence on the coagulation behaviors, HA coagulation in MgCl₂ solutions with a concentration from 0.2 to 2.0 mM was evaluated. Tris buffer, which shows negligible metal binding effect at 20 °C, was selected as the solvent.⁴⁵ Figure 4 shows that at a concentration lower than 1 mM, the $\langle R_h \rangle$ remained almost constant, while a rapid rise of $\langle R_h \rangle$ was observed when the MgCl₂ concentration exceeded 1.7 mM. Compared with Figure 1, a much lower concentration of Mg²⁺ than Na⁺ could induce a drastic HA coagulation. From the Schulze-Hardy rule, the theoretical coagulation value is determined by the valency of the ions, which are oppositely

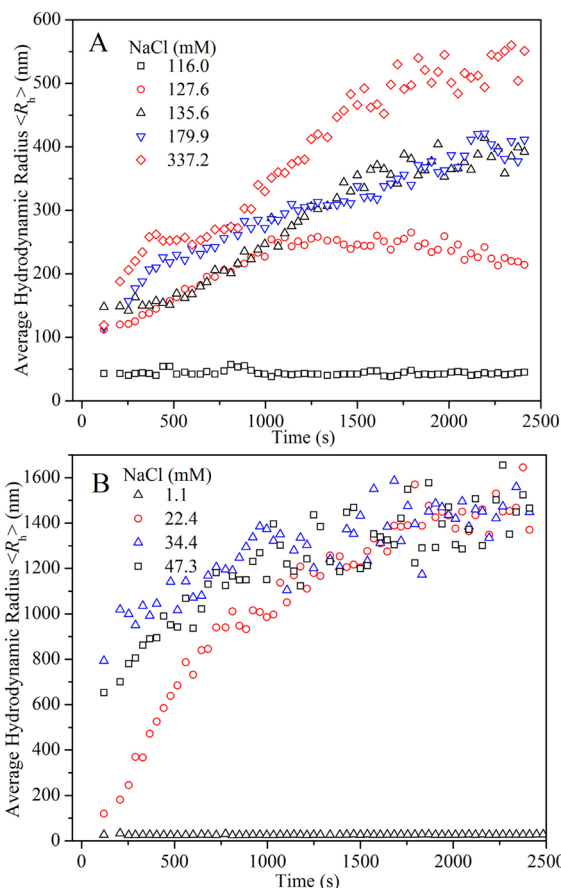


Figure 3. Coagulation profiles of HA aggregates as a function of time over a range of (A) NaCl concentration from 116.0 mM to 453.3 mM at pH 10.0; and (B) NaCl concentration from 1.1 mM to 47.3 mM at pH 3.6.

charged to the colloidal particles.³⁴ (proportional to z^{-6} for particles, where z is the valence of cation)

$$M^+ : M^{2+} = 1^6 : \left(\frac{1}{2}\right)^6 \quad (1)$$

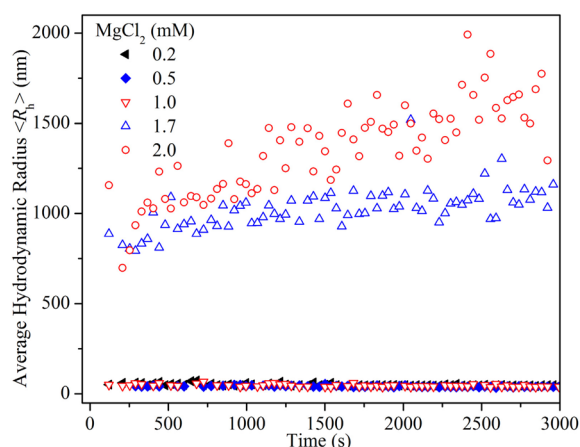
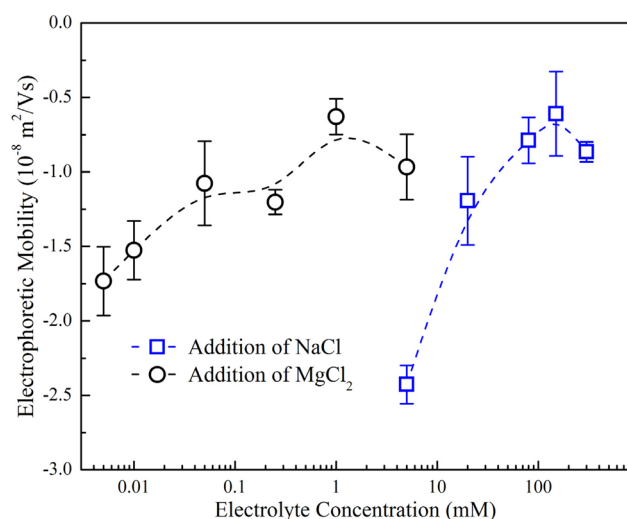
The coagulation value of NaCl in the same buffer was in a range of 61.3–84.4 mM. In contrast, the coagulation value of MgCl₂ was calculated to be within 0.96 and 1.33 mM, which is in the range of the experimental data. The final maximum aggregate $\langle R_h \rangle$ was 1583 ± 131 nm in the presence of 2 mM MgCl₂. The dose of 2 mM Mg²⁺ caused an intense fluctuating radius in the final coagulation process (Figure 4), which is similar to the later coagulation stages shown in Figure 2.

Electrophoretic Mobilities of HA. Figure 5 presents the electrophoretic mobilities of HA in pH 7.1 Tris-HCl buffer over a range of NaCl and MgCl₂ concentrations. All the samples were negatively charged. As the NaCl concentration was increased from 5 to 100 mM, the electrophoretic mobility tended to be less negative as a result of charge screening effect. This phenomenon has been commonly observed for other colloidal aggregates.^{32,33} Figure 5 also shows that, compared to monovalent Na⁺, Mg²⁺ was much more effective in reducing the electrophoretic mobility of the HA aggregates.

TEM Observations. TEM imaging illustrates that HAs were colloidal-sized macromolecules with variable structures at different pHs. Their macromolecules were predominantly globular aggregates with ring-like structure of rough periphery

Table 2. Typical Coagulation Rates and the Final Maximum Aggregate $\langle R_h \rangle$

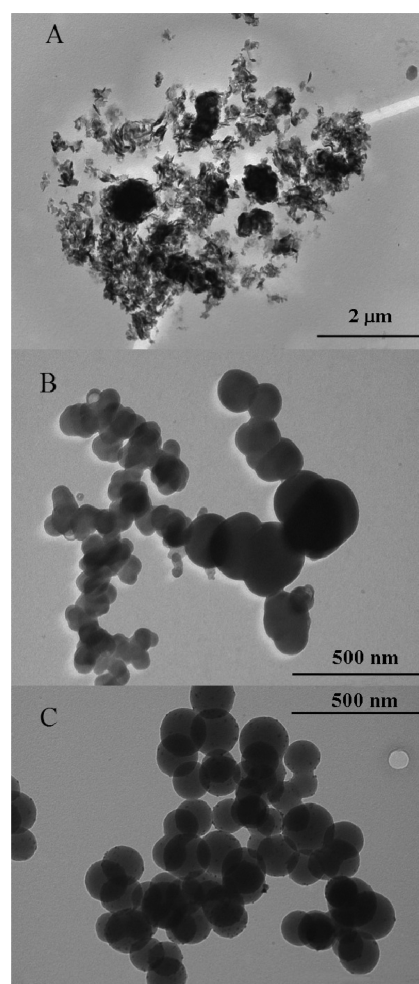
pH	typical coagulation rates (data from 120 to 820 s)				final maximum aggregate $\langle R_h \rangle$		electrolyte
	$(d\langle R_h \rangle/dt)$ (nm/s)	$\langle R_h \rangle$ at 120 s (nm)	adjusted R^2	corresponding conc. (mM)	average of last ten $\langle R_h \rangle$ (nm)	corresponding conc. (mM)	
3.6	1.34 ± 0.05	120	0.979	22.4	1452 ± 88	22.4	NaCl
7.1	0.90 ± 0.06	171	0.938	119.0	1283 ± 60	178.7	
10.0	0.15 ± 0.01	113	0.982	127.6	528 ± 24	337.2	
7.1					1583 ± 131	2.0	MgCl ₂

**Figure 4.** Coagulation profiles of HA aggregates as a function of time over a range of MgCl₂ concentration from 0.2 mM to 2 mM at pH 7.1.**Figure 5.** Electrophoretic mobilities of HA solution as a function of electrolyte concentration in pH 7.1 Tris-HCl buffer. Each data point represents the mean electrophoretic mobility. Error bars represent standard deviations.

at pH 5.26 (Figure 6A), similar to the HS morphology observed at $\text{pH } 3.0 \pm 1.0$.⁴⁶ As pH was increased to 7.00, the periphery became less rough and more globule-like. The HA macromolecules changed to smooth spherical particles with a radius of approximately 50 nm (Figure 6C) at pH 10.00. This is consistent with the average hydrodynamic radius (52 ± 2 nm) determined by DLS.

DISCUSSION

HA Coagulation Mechanisms in Electrolyte Solutions. The coagulation of colloidal HA is of great importance in

**Figure 6.** TEM images of HA at pH: (A) 5.26; (B) 7.00; and (C) 10.00 after instant freezing in liquid nitrogen, followed by lyophilization.

understanding the transport and fate of pollutants.^{1,2,4} However, the coagulation kinetics of HA and the influences of solution chemistry have not been thoroughly understood. For both natural and engineered aquatic systems, common discrepancy in electrolyte might result in different solution chemistry. Thus, typical monovalent and divalent electrolytes, that is, NaCl and MgCl₂, were selected to study their impacts on the HA coagulation.

HAs are a basically heterogeneous mixture of polyelectrolytic organic molecules and exhibit a continuous distribution of molecular and structural properties. Since they show polydispersity and mass fractal features in solution, the interpretation of DLS data might be complicated.^{7,17} However, polydispersity is found to have no significant effect on the aggregation of colloids and calculated D_p .^{47,48} Power-law

coagulation kinetics at pH 7.1 was observed at higher NaCl concentrations (94.4 to 380.5 mM) (Figure 1 and Table 1), which is a typical feature for the DLCA regime. However, the coagulation profiles in the presence of 84.4 mM NaCl could not be well fitted by neither DLCA model nor RLCA model. The total interaction potential between soft clusters (e.g., HA and microgel particles) is different from that for rigid nanoparticles, where interpenetration effect, for example, osmotic and elastic potentials, should be taken into account and the binding forces within the clusters might be weaker.^{49–51} Thus, when there is a finite interparticle attraction energy, for example, at a lower electrolyte concentration, unbinding and breaking of clusters would occur, resulting in reversible aggregation, that is, aggregates may dissociate spontaneously.^{49–52} Figure 1 shows that in the presence of 84.4 mM NaCl, $\langle R_h \rangle$ gradually increased in the early coagulation process, while remained almost unchanged after 2000 s. This could be explained by that at later coagulation stage, the formed clusters started to disaggregate and finally the aggregation and disaggregation rates reached a dynamic equilibrium. As the NaCl concentration was increased from 94.4 to 380.5 mM, the coagulation could be fitted by typical power-law kinetics well. In comparison, the modeled d_f values (Table 1) were larger than those for typical DLCA ($d_f = 1.85 \pm 0.1$)^{35–37} and other reported mass fractal dimensions of HS,³⁸ implying their relatively more compact structure. The possible explanation for the discrepancy in d_f might be the soft characters and lower rigidity of biological molecules compared to engineered colloids, which results in weaker clusters and restructuring of the colloids.^{50,51}

Effect of Mg^{2+} on HA Coagulation. HA colloids exhibit different coagulation behaviors induced by typical divalent electrolyte $MgCl_2$.^{32,33} The main difference between the coagulation behaviors of HAs and that of other nanoparticles (e.g., Ag nanoparticles and carbon nanotubes) is the disappearance of gradual increase in $\langle R_h \rangle$ at the early stage of agglomeration at pH 7.1 (Figure 4), implying that a rapid coagulation occurs instantly after the dose of Mg^{2+} . For engineered nanoparticles with rigid structures, the effect of dosing divalent cation Mg^{2+} is predominantly charge neutralization,³³ which is considerably different for HAs. The interactions between Mg^{2+} and HAs include (1) electrostatic interactions between Mg^{2+} and the negatively charged functional groups; and (2) complexation/bridging effect of carboxyl, phenolic groups with Mg^{2+} .^{1,5} Compared to monovalent cations, divalent cations can screen charges and reduce repulsion forces more effectively, which has been confirmed by the electrophoretic mobility measurements. Complexation of Mg^{2+} and HAs promotes the formation of micellar structure with intramolecular rearrangement, leading to an increased aggregate size, as evidenced in Figure 4 and Table 2. Bound divalent cations could form intra and/or intermolecular bridges between adjacent HA colloids, and as a result increase the attractive intermolecular forces. Thus, divalent Mg^{2+} is considered to be rapidly adsorbed onto the HA molecules, and the combined effects of charge screening, complexation as well as bridging facilitate coagulation of HAs in the presence of Mg^{2+} at a lower electrolyte concentration.

Effect of pH on HA Coagulation. The coagulation kinetics of HAs is also found to be pH dependent. HA colloids are stabilized by some weak forces such as dispersive hydrophobic interactions (i.e., van der Waals, π - π , and CH- π bondings) and hydrogen bonds.^{18,19,53} The latter is pro-

gressively more important at a low pH.⁵³ The dissociation degree of functional groups of biopolymer chains depends largely on the solution pH.^{54,55} The colloidal stabilities would be significantly different at different pHs as the electrostatic field is developed from proton dissociation of acidic groups.²¹ At pH 3.6, strong intermolecular hydrogen bonds hold HA molecules together. The presence of protonated -COOH is confirmed by the FTIR analysis (SI Figure S2). Thus, a rather low NaCl concentration would quickly induce the coagulation of HAs and form large macromolecular structure. With an increase in pH, the release of protons and dissociation of functional groups prevent the formation of hydrogen bonds and could leave the surface molecules more susceptible to detachment, leading to a relatively lower coagulation rate. At pH 10.0, an electrostatic repulsion may prevail over the molecules, as -COOH and phenolic -OH functional groups become fully negatively charged upon deprotonation and give rise to a continuous increase in the negative surface charge. Under such a circumstance, more counterions are needed to change the electrostatic equilibrium of HA colloids. Tombacz et al. reported that at a high pH, the functional groups of HAs are fully ionized and the charges linked by organic structures try to locate as far as possible from each other.⁵¹ This is responsible for the highest coagulation value in alkaline solution (between 116.0 mM and 127.6 mM). The contribution of hydrogen bonds may account for the significant pH-dependent variance observed in the final maximum aggregate $\langle R_h \rangle$ in Table 2.

Morphology of HA. DLS is a powerful technique for determining the size and size distribution of nanoparticles at microscale. By using DLS, the detailed coagulation information of HAs in solutions can be obtained. The DLS results may also be related with the TEM observations and give more efficient information on the morphology of HAs.^{46,56} HA macromolecules are predominantly globular aggregates with a ring-like structure of rough periphery at pH 5.26. The rough morphology and hydrogen forces make HAs more susceptible to be attached by other aggregates, resulting in higher coagulation rates. Smooth spherical particles are formed in alkaline solution due to relatively higher electrostatic repulsion forces.

Implications of This Work. Since the coagulation behaviors of HAs strongly influence the pollutant adsorption, distribution and removal in environmental remediation, this work is of high significance. Our results show that the HA coagulation is dependent highly on solution chemistry. The surrounding pH, protonation/deprotonation states of functional groups as well as metal complexation/bridging effects could influence the coagulation behaviors of HAs. The evolutions of HA colloids are attributed mainly to the physicochemical changes of the molecules. Nucleophilic reactive groups, for example, -COOH, phenolic-, and aliphatic -OH, in HAs and fulvic acids are reported to adsorb and produce chemical changes to different contaminants, for example, metals, pesticides, and nanoparticles.^{1,2,4} For example, at a lower pH, more atrazine (a common pesticide) was found to bind with HAs and the rapid formation of HA aggregates could help temporarily trap more atrazine, thus reducing its toxic properties.⁵⁷ An analysis on the HA coagulation processes in electrolyte solutions may also provide insights into HAs-induced membrane fouling in seawater desalination and in the processes associated with filtration of natural water under seasonal eutrophication.^{24–26} Therefore, the results of this work might facilitate a better understanding of the coagulation

behaviors of humic aggregates in both natural and engineered aqueous systems.

■ ASSOCIATED CONTENT

■ Supporting Information

X-ray photoelectron spectra of HAs; high resolution 1 s XPS spectra of C, O, and N in HAs; binding energies (eV) and assignment/quantization of XPS spectral bands; FTIR spectra of HAs at pH 1.7–10.04; infrared absorption bands of HA; titration results for HAs calculated with PROTOFIT; negative charge of HAs as a function of pH; parameters for proton binding in the NICA-Donnan model; HA coagulation observations. This information is available free of charge via the Internet at <http://pubs.acs.org/>.

■ AUTHOR INFORMATION

Corresponding Author

*E-mail: xdye@ustc.edu.cn (X.-D. Y.); hqyu@ustc.edu.cn (H.-Q. Y.).

Author Contributions

Long-Fei Wang and Ling-Ling Wang contributed equally to this work.

Notes

The authors declare no competing financial interest.

■ ACKNOWLEDGMENTS

We thank Dr. Ming-Quan Yan from Department of Environmental Engineering, College of Environmental Sciences and Engineering, Peking University for his valuable review comments. We also wish to thank the Natural Science Foundation of China (51129803 and 21274140) and the Program for Changjiang Scholars and Innovative Research Team in University, China for the partial support of this work.

■ REFERENCES

- (1) Stevenson, F. J., *Humus Chemistry: Genesis, Composition, Reactions*, 2nd ed.; John Wiley & Sons: New York, 1994.
- (2) Aiken, G. R.; McKnight, D. M.; Wershaw, R. L.; MacCarthy, P., *Humic Substances in Soil, Sediment and Water, Geochemistry, Isolation and Characterization*; John Wiley & Sons: New York, 1985.
- (3) Avena, M. J.; Wilkinson, K. J. Disaggregation kinetics of a peat humic acid: Mechanism and pH effects. *Environ. Sci. Technol.* **2002**, *36*, 5100–5105.
- (4) Jones, M. N.; Bryan, N. D. Colloidal properties of humic substances. *Adv. Colloid Interface Sci.* **1998**, *78*, 1–48.
- (5) Engebretson, R. R.; von Wandruszka, R. Kinetic aspects of cation-enhanced aggregation in aqueous humic acids. *Environ. Sci. Technol.* **1998**, *32*, 488–493.
- (6) Balnois, E.; Wilkinson, K. J.; Lead, J. R.; Buffle, J. Atomic force microscopy of humic substances: Effects of pH and ionic strength. *Environ. Sci. Technol.* **1999**, *33*, 3911–3917.
- (7) Senesi, N.; Rizzi, F. R.; Dellino, P.; Acquafredda, P. Fractal humic acids in aqueous suspensions at various concentrations, ionic strengths, and pH values. *Colloids Surf., A* **1997**, *127*, 57–68.
- (8) Lead, J. R.; Wilkinson, K. J.; Starchev, K.; Canonica, S.; Buffle, J. Determination of diffusion coefficients of humic substances by fluorescence correlation spectroscopy: Role of solution conditions. *Environ. Sci. Technol.* **2000**, *34*, 1365–1369.
- (9) Hosse, M.; Wilkinson, K. J. Determination of electrophoretic mobilities and hydrodynamic radii of three humic substances as a function of pH and ionic strength. *Environ. Sci. Technol.* **2001**, *35*, 4301–4306.
- (10) Fetsch, D.; Hradilova, M.; Mendez, E. M. P.; Havel, J. Capillary zone electrophoresis study of aggregation of humic substances. *J. Chromatogr., A* **1998**, *817*, 313–323.

(11) Smejkalova, D.; Piccolo, A. Aggregation and disaggregation of humic supramolecular assemblies by NMR diffusion ordered spectroscopy (DOSY-NMR). *Environ. Sci. Technol.* **2008**, *42*, 699–706.

(12) Shinozuka, N.; Lee, C. Aggregate formation of humic acids from marine sediments. *Mar. Chem.* **1991**, *33*, 229–241.

(13) Terashima, M.; Fukushima, M.; Tanaka, S. Influence of pH on the surface activity of humic acid: Micelle-like aggregate formation and interfacial adsorption. *Colloids Surf., A* **2004**, *247*, 77–83.

(14) Pinheiro, J. P.; Mota, A. M.; Oliveira, J. M. R.; Martinho, J. M. G. Dynamic properties of humic matter by dynamic light scattering and voltammetry. *Anal. Chim. Acta* **1996**, *329*, 15–24.

(15) Reid, P. M.; Wilkinson, A. E.; Tipping, E.; Jones, M. N. Aggregation of humic substances in aqueous-media as determined by light scattering methods. *J. Soil Sci.* **1991**, *42*, 259–270.

(16) Baigorri, R.; Fuentes, M.; Gonzalez-Gaitano, G.; Garcia-Mina, J. M. Analysis of molecular aggregation in humic substances in solution. *Colloids Surf., A* **2007**, *302*, 301–306.

(17) Ren, S. Z.; Tombacz, E.; Rice, J. A. Dynamic light scattering from power-law polydisperse fractals: Application of dynamic scaling to humic acid. *Phys. Rev. E* **1996**, *53*, 2980–2983.

(18) Conte, P.; Piccolo, A. Conformational arrangement of dissolved humic substances. Influence of solution composition on associations of humic molecules. *Environ. Sci. Technol.* **1999**, *33*, 1682–1690.

(19) Sutton, R.; Sposito, G. Molecular structure in soil humic substances: The new view. *Environ. Sci. Technol.* **2005**, *39*, 9009–9015.

(20) Wershaw, R. L. Molecular aggregation of humic substances. *Soil Sci* **1999**, *164*, 803–813.

(21) Tombacz, E. Colloidal properties of humic acids and spontaneous changes of their colloidal state under variable solution conditions. *Soil Sci.* **1999**, *164*, 814–824.

(22) Tombacz, E.; Meleg, E. A theoretical explanation of the aggregation of humic substances as a function of pH and electrolyte concentration. *Org. Geochem.* **1990**, *15*, 375–381.

(23) Stumm, W.; Morgan, J. J., *Aquatic Chemistry: Chemical Equilibria and Rates in Natural Waters*; John Wiley & Sons: New York, 1996.

(24) Hong, S. K.; Elimelech, M. Chemical and physical aspects of natural organic matter (NOM) fouling of nanofiltration membranes. *J. Membr. Sci.* **1997**, *132*, 159–181.

(25) Lee, S.; Elimelech, M. Relating organic fouling of reverse osmosis membranes to intermolecular adhesion forces. *Environ. Sci. Technol.* **2006**, *40*, 980–987.

(26) Wolfe, A. P.; Kaushal, S. S.; Fulton, J. R.; McKnight, D. M. Spectrofluorescence of sediment humic substances and historical changes of lacustrine organic matter provenance in response to atmospheric nutrient enrichment. *Environ. Sci. Technol.* **2002**, *36*, 3217–3223.

(27) Kang, K. H.; Shin, H. S.; Park, H. Characterization of humic substances present in landfill leachates with different landfill ages and its implications. *Water Res.* **2002**, *36*, 4023–4032.

(28) Rex, M. C. D.; Daphne, C. E.; William, H. E.; Kenneth, M. J. *Data for Biochemical Research*; Clarendon Press: Oxford, 1986.

(29) Turner, B. F.; Fein, J. B. Proffit: A program for determining surface protonation constants from titration data. *Comput. Geosci.* **2006**, *32*, 1344–1356.

(30) Wu, C.; Zhou, S. Q. First observation of the molten globule state of a single homopolymer chain. *Phys. Rev. Lett.* **1996**, *77*, 3053–3055.

(31) Chu, B., *Laser Light Scattering*, 2nd ed.; Academic Press: New York, 1991.

(32) Chen, K. L.; Elimelech, M. Influence of humic acid on the aggregation kinetics of fullerene (C-60) nanoparticles in monovalent and divalent electrolyte solutions. *J. Colloid Interface Sci.* **2007**, *309*, 126–134.

(33) Huynh, K. A.; Chen, K. L. Aggregation kinetics of citrate and polyvinylpyrrolidone coated silver nanoparticles in monovalent and divalent electrolyte solutions. *Environ. Sci. Technol.* **2011**, *45*, 5564–5571.

(34) Verwey, E. J. W.; Overbeek, J. T. G. *Theory of the Stability of Lyophobic Colloids*; Elsevier: Amsterdam, 1948.

- (35) Lin, M. Y.; Lindsay, H. M.; Weitz, D. A.; Ball, R. C.; Klein, R.; Meakin, P. Universality in colloid aggregation. *Nature* **1989**, *339*, 360–362.
- (36) Weitz, D. A.; Huang, J. S.; Lin, M. Y.; Sung, J. Limits of the fractal dimension for irreversible kinetic aggregation of gold colloids. *Phys. Rev. Lett.* **1985**, *54*, 1416–1419.
- (37) Lin, M. Y.; Lindsay, H. M.; Weitz, D. A.; Klein, R.; Ball, R. C.; Meakin, P. Universal diffusion-limited colloid aggregation. *J Phys: Condens Matter* **1990**, *2*, 3093–3113.
- (38) Rice, J. A.; Lin, J. S. Fractal nature of humic materials. *Environ. Sci. Technol.* **1993**, *27*, 413–414.
- (39) Kozlov, G. V.; Zaikov, G. E.; Novikov, V. U. *Fractal Analysis of Polymers: From Synthesis to Composites*; Nova Science Publisher: Hauppauge, NY, 2003.
- (40) Omoike, A.; Chorover, J. Spectroscopic study of extracellular polymeric substances from *Bacillus subtilis*: Aqueous chemistry and adsorption effects. *Biomacromolecules* **2004**, *5*, 1219–1230.
- (41) Dewit, J. C. M.; Vanriemsdijk, W. H.; Koopal, L. K. Proton binding to humic substances. 1. Electrostatic effects. *Environ. Sci. Technol.* **1993**, *27*, 2005–2014.
- (42) Ritchie, J. D.; Perdue, E. M. Proton-binding study of standard and reference fulvic acids, humic acids, and natural organic matter. *Geochim. Cosmochim. Acta* **2003**, *67*, 85–96.
- (43) Palmer, N. E.; von Wandruszka, R. Dynamic light scattering measurements of particle size development in aqueous humic materials. *Fresenius J. Anal. Chem.* **2001**, *371*, 951–954.
- (44) Zhang, W.; Crittenden, J.; Li, K. G.; Chen, Y. S. Attachment efficiency of nanoparticle aggregation in aqueous dispersions: Modeling and experimental validation. *Environ. Sci. Technol.* **2012**, *46*, 7054–7062.
- (45) Good, N. E.; Winget, G. D.; Winter, W.; Connolly, T. N.; Izawa, S.; Singh, R. M. M. Hydrogen ion buffers for biological research. *Biochemistry* **1966**, *5*, 467–477.
- (46) Myneni, S. C. B.; Brown, J. T.; Martinez, G. A.; Meyer-Ilse, W. Imaging of humic substance macromolecular structures in water and soils. *Science* **1999**, *286*, 1335–1337.
- (47) Dimon, P.; Sinha, S. K.; Weitz, D. A.; Safinya, C. R.; Smith, G. S.; Varady, W. A.; Lindsay, H. M. Structure of aggregated gold colloids. *Phys. Rev. Lett.* **1986**, *57*, 595–598.
- (48) Bushell, G.; Amal, R. Fractal aggregates of polydisperse particles. *J. Colloid Interface Sci.* **1998**, *205*, 459–469.
- (49) Cheng, H.; Wu, C.; Winnik, M. A. Kinetics of reversible aggregation of soft polymeric particles in dilute dispersion. *Macromolecules* **2004**, *37*, 5127–5129.
- (50) Fernandez-Nieves, A.; Fernandez-Barbero, A.; Vincent, B.; de las Nieves, F. J. Reversible aggregation of soft particles. *Langmuir* **2001**, *17*, 1841–1846.
- (51) Meakin, P.; Jullien, R. The effects of restructuring on the geometry of clusters formed by diffusion-limited, ballistic, and reaction-limited cluster cluster aggregation. *J. Chem. Phys.* **1988**, *89*, 246–250.
- (52) Jeffrey, G. C.; Ottewill, R. H. Reversible aggregation Part 2. Kinetics of reversible aggregation. *Colloid Polym. Sci.* **1990**, *268*, 179–189.
- (53) Piccolo, A. The supramolecular structure of humic substances. *Soil Sci.* **2001**, *166*, 810–832.
- (54) Engbretson, R. R.; Amos, T.; von Wandruszka, R. Quantitative approach to humic acid associations. *Environ. Sci. Technol.* **1996**, *30*, 990–997.
- (55) Wang, L. L.; Wang, L. F.; Ren, X. M.; Ye, X. D.; Li, W. W.; Yuan, S. J.; Sun, M.; Sheng, G. P.; Yu, H. Q.; Wang, X. K. pH dependence of structure and surface properties of microbial EPS. *Environ. Sci. Technol.* **2012**, *46*, 737–744.
- (56) Baalousha, M.; Motelica-Heino, M.; Le Coustumer, P. Conformation and size of humic substances: Effects of major cation concentration and type, pH, salinity, and residence time. *Colloids Surf., A* **2006**, *272*, 48–55.
- (57) Martinetto, L.; Vieira, E. M.; Sposito, G. Mechanism of atrazine sorption by humic acid—a spectroscopic study. *Environ. Sci. Technol.* **1994**, *28*, 1867–1873.